Solid State Science and Technology, Vol. 24, No 2 (2016) 239-252
ISSN 0128-7389 | *http://journal.masshp.net*

EFFECT OF SrO CONTENT ON THE STRUCTURE AND ELASTIC BEHAVIOR OF $xSrO\text{-}(90\text{-}x)B_2O_3\text{-}2CeO_2\text{-}8Al_2O_3$ GLASS

Nurul Syahidah Sabri, A.K. Yahya and Mahesh Kumar Talari

Faculty of Applied Sciences, Universiti Teknologi MARA, 40450 Shah Alam, Selangor, Malaysia

Corresponding author: talari@gmail.com

ABSTRACT

Strontium cerium aluminium borate glass samples with composition $xSrO\text{-}(90\text{-}x)B_2O_3\text{-}2CeO_2\text{-}8Al_2O_3$ (x=25, 30, 35, 40, 45 and 50 mol%) were prepared by melt-quenching method to investigate the elastic behavior and phase formation. XRD data showed amorphous and mixed crystalline/amorphous phases for the samples with SrO concentration $x \leq 35$ mol% and $x > 35$ mol%, respectively. FESEM image and EDX analysis revealed that the samples contained Ce-rich crystalline phase and Ce depleted glass phase. FTIR analysis showed that the glass consisted of BO_4 and BO_3 structural units. Addition of SrO has resulted in increased ultrasonic velocities, longitudinal modulus (C_L), shear modulus (μ), bulk Modulus (K), Young's modulus (Y) and hardness (H) at $x \leq 35$ mol%. The increase in the elastic moduli indicates increase of network rigidity of the glass system, related to the borate anomaly where the coordination number increased with the addition of SrO. Decrease in elastic moduli related to formation of NBO and formation of grain / phase boundaries due to mixed crystalline / amorphous phases at higher SrO addition. Quantitative analysis of ultrasonic data using the bulk compression and ring deformation models showed reduction in the ratio of calculated bulk modulus to the experimental bulk modulus, K_{bc}/K_e indicating decreased ring deformation in borate anomaly region.

Keywords: Borate Anomaly; Immiscibility; Elastic properties; Rare earth; Doped borate glass;

INTRODUCTION

Borate glasses containing alkali or alkaline oxide have gained great attention among researchers and technologists for many years. Borate glasses display interesting properties, related to borate anomaly phenomenon, which can be tuned by altering the concentration of alkaline and alkaline earth modifiers. Several attempts have been made to understand the structure of these glasses and their relationship with properties [1]. Ultrasonic characterization technique could be employed to understand the structural aspects of the glass network by monitoring ultrasonic velocities and moduli of glasses. Changes that occur in the glass network due to modifier addition could be directly

detected by ultrasonic measurements, besides density and molar volume, as it could provide information related to the forces between the atoms or ions in the glass network [2]. Besides alkali and alkaline earth doping, Ce and Al addition into borate glass could also modify the glass network by converting BO_3 groups into tetrahedral BO_4 units [3-4]. Hence, it would be interesting to investigate elastic properties of SrO-B_2O_3-CeO_2-Al_2O_3 glass system by varying SrO concentration to further elucidate anomalous behaviour of this glass system. There have been many reports published related to emission properties of rare earth (RE)-borate glass [1, 3–6]. However, reports on elastic properties of alkaline earth doped RE-borate glasses are limited. Thus, the present paper aims to investigate the effect of SrO on structure of $xSrO$-$(90-x)B_2O_3$-$2CeO_2$-$8Al_2O_3$ glass system in terms of the density, the elastic behavior and the ring diameter.

EXPERIMENTAL

Material and Methods

Glass samples of the system $xSrO$-$(90-x)B_2O_3$-$2CeO_2$-$8Al_2O_3$ (x=25, 30, 35, 40, 45 and 50 mol%) were prepared using melt-quenching method. Analytical grade strontium carbonate ($SrCO_3$), cerium oxide (CeO_2), aluminium oxide (Al_2O_3) and boron oxide (B_2O_3) were used as starting materials for this work. Precursor powders of the materials were mixed and ground continuously for 1 hour using agate mortar and pestle to achieve good homogeneity. After mixing the powders, the mixture was placed in a porcelain crucible and melted for 1 hour in a box furnace at 1100°C. The molten glass was then quenched to 300°C in a stainless steel mould and maintained at this temperature for 1 hour. X-Ray Diffraction (XRD) data was collected using Panalytical X-Ray diffractometer to investigate the structure of the glass samples. Infrared (IR) absorption spectra of glass powder samples were recorded using a Perkin Elmer model Spectrum One FTIR spectrometer. Each powder sample was mixed with KBr in a fixed ratio of 1:80 and pressed into a pellet using a hand press. The spectrometer covered the range 400-1600 cm^{-1} with 4 cm^{-1} resolution. A Zeiss Supra 40VP microscope was used to obtain FESEM images and perform EDX with an acceleration voltage of 10 kV to analyze microstructure of immiscible glasses.

Archimedes principle was used to obtain density (ρ) of the glass samples with toluene as the immersion liquid at room temperature using the equation

$$\rho = \left(\frac{W}{W-W_b}\right)\rho_b \qquad \text{(Eq.1)}$$

where W is the glass sample weight in air, W_b is the glass sample weight in toluene and ρ_b is the density of toluene (0.865 g/mL). For ultrasonic velocity measurement of glass samples, RITEC model 5000 ultrasonic system was used. All the measurements were taken at 5 MHz in both longitudinal and shear modes by applying the pulse-echo technique at room temperature. Elastic moduli such as longitudinal (C_L), shear (μ), bulk (K), Young's (Y) and mean velocity (v_m), Debye temperature (θ_D), Poisson's ratio (σ),

hardness (H) were obtained from the experimental values of density (ρ), molar volume (V_a), longitudinal velocity (v_L) and shear velocity (v_S) as described elsewhere [7].
A bulk compression model assumes that an isotropic deformation changes the network bond lengths without any change in bond angle and depends on bond stretching force constant (F) [8]. This bulk compression model was first proposed by Bridge et al. [9] for the study of single-component oxide glass where the ideal bulk modulus (K_{bc}) is given by

$$K_{bc} = \frac{n_b r^2 F}{9} \qquad \text{(Eq. 2)}$$

where r is the bond length and F is the stretching force constant. This computed modulus is directly proportional to the number of network bonds per unit volume, n_b which is given by

$$n_b = \frac{n_f N_A}{V_a} \qquad \text{(Eq. 3)}$$

where n_f is the number of network bonds per glass formula unit, N_A is Avogadro's number and V_a is the molar volume of the glass.

This bulk compression model was further developed for polycomponent oxide glasses with i different types of network bonds [8]. Thus, equation can be written as

$$K_{bc} = \frac{N_A}{9V_a}\sum_i \left(x n_f F r^2\right)_i \qquad \text{(Eq. 4)}$$

where x is the mole fraction. The stretching force constant, F, is given by

$$F = \frac{1.7}{r^3} \qquad \text{(Eq. 5)}$$

As the coordination number of the boron varies from 3 to 4, the average coordination number of boron can be calculated using the formula [10]

$$n_{f_{ave}} = (4-3)x\mathrm{N}_4 + 3 \qquad \text{(Eq. 6)}$$

The average bond length of B_2O_3 ($r_{B_2O_3}$) when both 3 and 4 coordinated boron atoms exist in the glass can also be calculated using the formula [10]

$$r_{B_2O_3} = \left(r_{BO_4} + r_{BO_3}\right)x\mathrm{N}_4 + r_{BO_3} \qquad \text{(Eq. 7)}$$

The average ring size (ℓ) which is defined as the ring perimeter (number of bonds times the bond length divided by π) is given by

$$\ell = \left[0.0106\frac{\bar{F}}{K_{exp}}\right]^{0.26} \qquad \text{(Eq. 8)}$$

where K_{exp} is the experimental bulk modulus. $\bar{F}$ is the average stretching force constant

$$\bar{F} = \frac{\sum\left(x n_f F\right)_i}{\sum\left(x n_f\right)_i} \qquad \text{(Eq. 9)}$$

RESULTS AND DISCUSSION

Figure 1 presents the XRD patterns of $xSrO\text{-}(90\text{-}x)B_2O_3\text{-}2CeO_2\text{-}8Al_2O_3$ samples. Absence of sharp peaks in the XRD patterns of the samples at $x \leq 35$ mol% SrO confirmed the amorphous nature of the samples. However, as the SrO content increased ($x > 35$ mol%), the samples showed both crystalline and amorphous phases. The crystalline phase showed diffraction peaks corresponding to CeO_2–based Face-Centred lattice based on PCPDF Reference no. 81-0792. Previous report on CeO_2–Al_2O_3–PbO–B_2O_3 glass also showed partial crystallinity in XRD spectra [3]. Optical and back scattered electron (BSE) micrographs of $50SrO\text{-}40B_2O_3\text{-}2CeO_2\text{-}8Al_2O_3$ sample are shown in Figure 2. The sample containing 50 mol% SrO showed two distinctive layers in their appearance, white opaque crystalline phase and dark transparant glass phase (Figure 2 (a)). BSE image (Figure 2 (b)) showed bright and darker regions identified as RE containing crystalline phase and glass phase. On further EDX analysis of bright and darker regions revealed Ce-rich (0.68 atomic %) and Ce depleted phases respectively. Higher alkali/alkaline earth oxide content in borate glass may result in liquid phase immiscibility where the liquid separates into two liquid phases [11]. In the current study, it can be suggested that the glass separated into alternative layers of two liquids before solidification, with one liquid enriched with Ce and the other Ce depleted. However, higher viscosity and closer density values of two liquids near freezing temperatures has resulted in incomplete separation into two layers before solidification. On further solidification below immiscibility boundary, Ce-rich liquid phase formed crystalline phase due to low glass forming ability and the other liquid transformed in to glass phase [12].

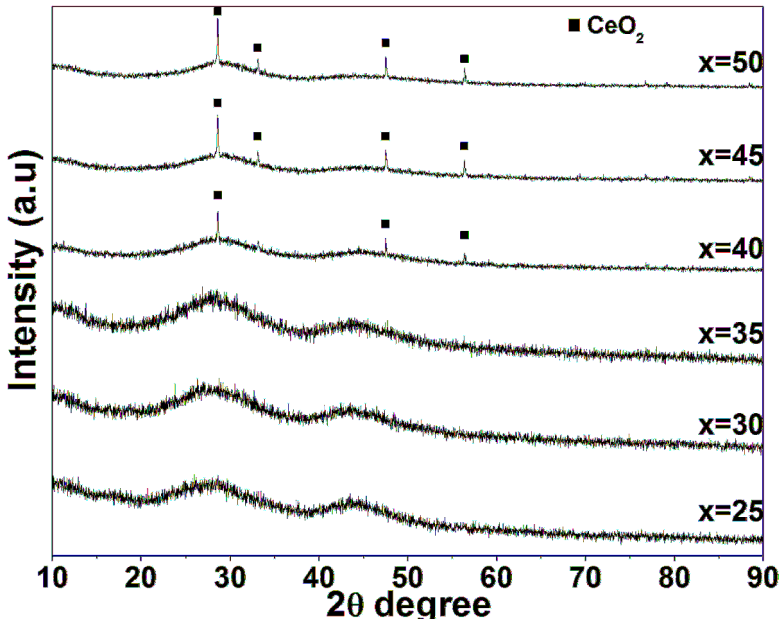

Figure 1: XRD patterns of $xSrO\text{-}(90\text{-}x)B_2O_3\text{-}2CeO_2\text{-}8Al_2O_3$ (x=25-50 mol%) samples

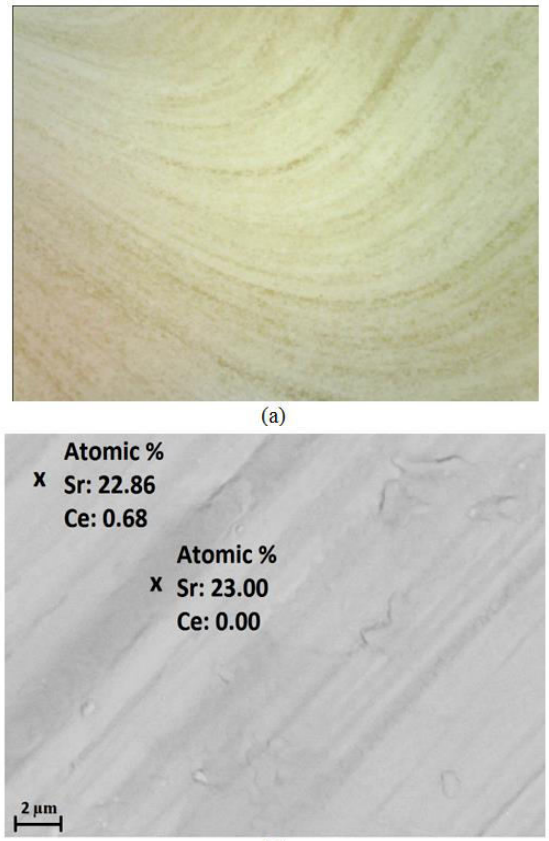

Figure 2: (a) Microscope image under 500 times magnification and (b) FESEM micrograph of immiscible $50SrO\text{-}40B_2O_3\text{-}2CeO_2\text{-}8Al_2O_3$ sample (back scattered electron image)

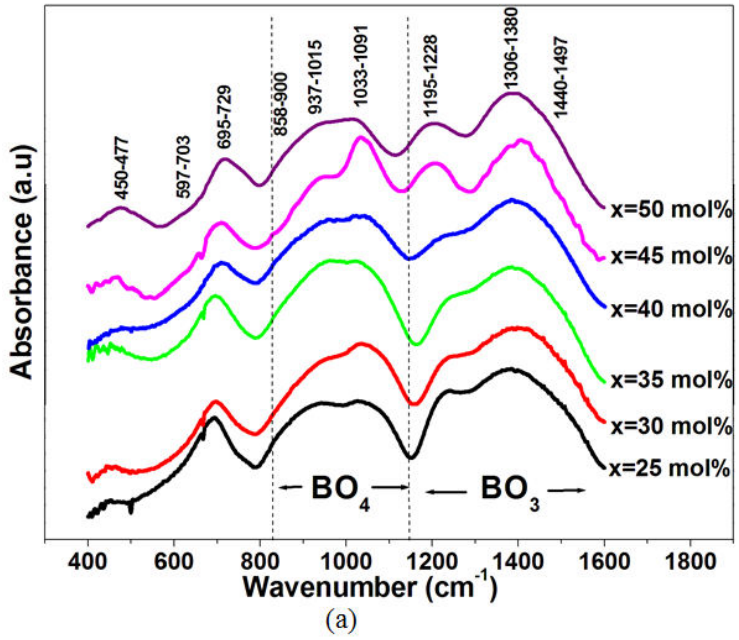

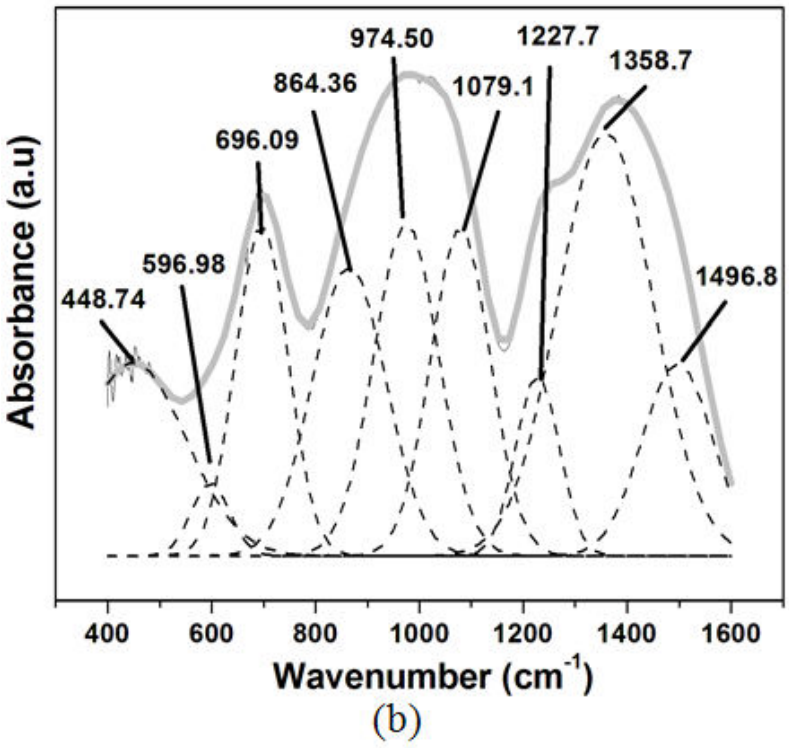

Figure 3: (a) IR spectra of $xSrO\text{-}(90\text{-}x)B_2O_3\text{-}2CeO_2\text{-}8Al_2O_3$ (x=25-50 mol%) samples & (b) Deconvoluted IR spectra of the $35SrO\text{-}65B_2O_3\text{-}2CeO_2\text{-}8Al_2O_3$ glass samples using a Gaussian type function

Figure 3 shows infrared (IR) absorption spectra for $xSrO\text{-}(90\text{-}x)B_2O_3\text{-}2CeO_2\text{-}8Al_2O_3$ (x=25-50 mol%) samples in the frequency range from 400 to 1600 cm^{-1} at room temperature. It is well known that borate glasses in general exhibit broad absorption peaks in three regions. Absorption in the region of 1500– 1200 cm^{-1} is due to stretching modes of $[BO_3]$ trigonal borons. The 1200–800 cm^{-1} region is attributed to the stretching modes of $[BO_4]^-$ tetrahedral borons and the 800–450 cm^{-1} is due to the various B–O–B bending modes. A deconvolution technique was used to get parameters such as individual band center (C) and its relative area (A), which is related to type of vibrations of individual structural group and concentration of these structural groups, respectively. Figure 3 shows the deconvolution of the spectrum for $35SrO\text{-}65B_2O_3\text{-}2CeO_2\text{-}8Al_2O_3$ glass sample. The deconvolution parameters and the assignments of the obtained bands for the glasses are given in Table 1. The parameter C of absorption bands (Table 1) can be used to calculate the fraction of the four coordinated boron atoms (N_4) in $xSrO\text{-}(90\text{-}x)B_2O_3\text{-}2CeO_2\text{-}8Al_2O_3$ (x=25-50 mol%) [13]:

$$N_4 = \frac{A_4}{A_4 + A_3} \qquad \text{(Eq. 10)}$$

where A_4 is the total area of BO_4 units which was taken from the areas of bands from 858-900, 937-1015 and 1033-1091 cm^{-1} while A_3 is the total area for BO_3 units component bands from 1195-1228, 1306-1380 and 1440-1497 cm^{-1}. As shown in Table 2, the value of N_4 increased as SrO content increased up to $x \leq 35$ mol% suggesting that the addition of SrO converts 3-coordinated boron to 4-coordinated boron at low concentration. This phenomenon is known as borate anomaly. Further addition of SrO above 35 mol% led to a decrease in N_4 value and this is due to the structural changes involving the conversions of the BO_4 into BO_3 structural units with increase in non bridging oxygen (NBO) formation [13].

Table 1: Wavenumbers and their assignments for IR spectra of $xSrO-(90-x)B_2O_3-CeO_2-8Al_2O_3$ samples

x = 25		x = 30		x = 35		x = 40		x = 45		x = 50		Assignments
C	A	C	A	C	A	C	A	C	A	C	A	
450	2.1	458	1.9	449	49.7	469	7.4	457	1.1	477	8.3	Angle's modification of the B-O-B linkage [13-14] Ring angle bending (B-O-B) [15] Vibrations of cerium cations [4]
653	37.1	681	20.6	597	6.9	703	97.8	702	0.8	702	17.7	O−B−O bond bending vibrations [13]
695	14.9	699	12.6	696	42.5	712	24.7	712	5.8	729	19.1	Bending vibrations of B-O-B [5, 13,16-17] Stretching vibrations of Al–O bonds in AlO_6 groups [3]
900	54.3	885	35.4	864	52.6	866	61.7	863	7.4	858	28.2	B-O stretch in BO_4 units from tri-, tetra- and penta-borate group [13, 18]
1015	28.7	994	42.2	975	52.6	943	35.5	944	8.1	937	35.7	B-O stretch in BO_4 units from di-borate groups [13, 19-20]
1091	22.8	1083	30.7	1079	47.7	1046	168.3	1047	11.6	1033	54.6	B-O stretch in BO_4 units from tri-, tetra- and penta-borate group [13, 18]
1215	18.5	1223	10.8	1228	20.0	1210	38.4	1195	16.2	1198	69.5	Stretching in $B–O^-$ bonds of trigonal BO_3 units from metaborate, pyroborate, and orthoborate groups [6, 13, 19-21]
1320	68.5	1306	64.2	1359	98.0	1312	111.8	1380	14.7	1355	60.0	
1477	77.4	1461	90.4	1497	33.1	1440	208.1	1470	13.7	1462	74.3	

Table 2: Values of fraction of the four coordinated boron atoms (N_4) for xSrO-(90-x)B_2O_3-2CeO_2-8Al_2O_3 (x=25-50 mol%) samples

x (mol%)	N_4
25	0.3918
30	0.3959
35	0.5036
40	0.4255
45	0.3782
50	0.3677

Figure 4 (a) depicts the composition dependence of the density (ρ) and molar volume (V_a) for xSrO-(90-x)B_2O_3-2CeO_2-8Al_2O_3 samples where ρ increased and V_a decreased as SrO content increased. The increase in ρ could be due to the replacement of lower molecular mass of B_2O_3 (69.62 g mol^{-1}) with greater molecular mass of SrO (103.62 g mol^{-1}) [10]. The rate of increase in ρ is higher between x=35 and x=40 mol% which may be associated with the phase changes from amorphous to mixed crystalline / amorphous phase [22]. In Figure 4 (a), V_a is observed to decrease monotonously at x ≤ 35 mol% and could be attributed to two factors, the formation of tetraborate (BO_4) structures and occupation of interstitial sites by SrO ions. Formation of mixed crystalline and amorphous phase at x > 35 mol% gives lower value in V_a compared to amorphous phase (x ≤ 35 mol%) as amorphous structure has more free volume that is characteristic of randomly packed structure compared mixed crystalline/amorphous structure. Simultaneous formation of NBO atoms and formation of crystalline phase would have resulted in constant V_a at x ≥ 45 mol%.

Figure 4 (b) shows that longitudinal velocities (v_L) and shear velocities (v_S) increased up to x ≤ 35 mol% and decreased for x > 35 mol% of SrO content in xSrO-10PbO-(90-x)B_2O_3 samples. The changes in ultrasonic velocities could be correlated with the structural changes of borate glass system with SrO addition. The addition of SrO to B_2O_3 network creates [BO_4] units and leads to increase in the network dimensionality and connectivity [2]. As can be seen from Figure 4 (b), maximum values of ultrasonic velocities (v_L and v_S) is at x = 35 mol%, correlated with N_4 value, suggesting that borate anomaly phenomenon occurs in the range of x ≤ 35 mol%. At higher SrO addition, formation of NBO and two phase microstructure with grain/phase boundaries might have contributed towards the decreased velocities.

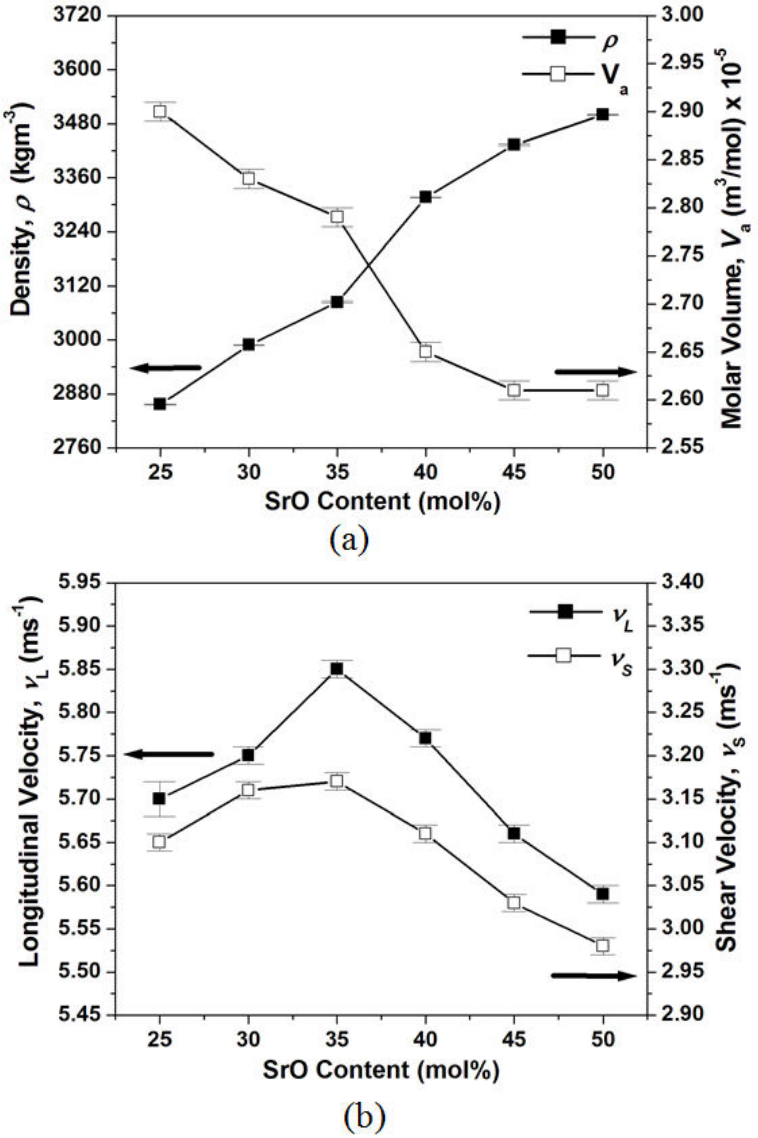

Figure 4: Plot of (a) density (ρ) and molar volume (V_a) & (b) longitudinal velocity (v_L) and shear velocity (v_S) for xSrO-(90-x)B_2O_3-2CeO_2-8Al_2O_3 (x=25-50 mol%) samples

Figure 5 (a) shows the variation of longitudinal modulus (C_L) and shear modulus (μ) for xSrO-10PbO-(90-x)B_2O_3 samples. Both these moduli increased up to x ≤ 40 mol% and then slightly decreased for x > 40 mol% SrO. Increase in C_L and μ up to 35 mol% could be due to increase in rigidity/stiffness and network connectivity as a result of conversion of BO_3 units to BO_4 units of boron [2]. At x=40 mol%, C_L and μ continued to increase which could be due to formation of mixed crystalline / amorphous phase induced by SrO addition for x > 35 mol%. The elastic stiffness/rigidity is usually larger in crystalline region compared to amorphous due to stronger intermolecular bond [23]. Slight decrease at x > 40 mol% of C_L and μ may be due to competition between increase number of NBO and formation of mixed crystalline/amorphous phase.

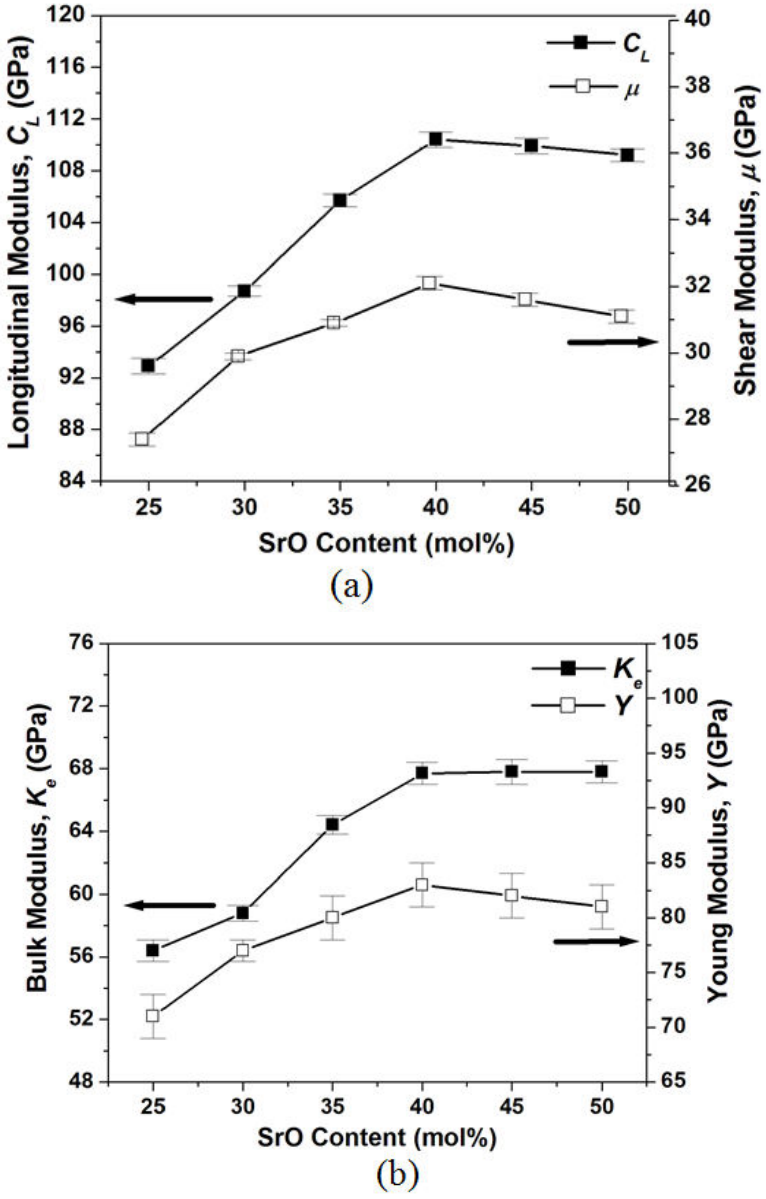

Figure 5: Plot of (a) longitudinal modulus (C_L) and shear modulus (μ) & (b) bulk modulus (K) and Young's modulus (Y) for xSrO-(90-x)B_2O_3-2CeO_2-8Al_2O_3 (x=25-50 mol%) samples

Bulk modulus (K_e) is the resistance of a material to compression involving change in volume [24]. As shown in Figure 5 (b), K_e is seen to increase with SrO addition for all the samples and did not show any decrease at higher SrO concentrations (mixed crystalline / amorphous phase region). According to equation of K_e [7], the behaviour of K_e is influenced by C_L and μ moduli. The increase in bulk modulus could be attributed

to the larger increase in C_L value (13.78%) compared to the increase in μ value (12.77%) for x ≤ 40 mol% SrO. However, the change in K_e is almost negligible for x > 40 mol% SrO. This could be attributed to interstitial occupation by Sr^{2+} and formation of mixed crystalline and amorphous phase in the borate structure. Consequently, the borate structure compression is tougher although the number of NBO formation increases. This could be further confirmed by the changes in molar volume (Figure 4 (a)) where molar volume is inversely proportional to bulk modulus. The behaviour of Y shows a similar trend with the C_L and μ as shown in Figure 6 (b) which shows that the behaviour of Y was influenced by the behaviour in both C_L and μ.

Poisson's ratio (σ) is the ratio between lateral and longitudinal strains produced by materials under stress [25]. The values of σ are in the range of 0.282-0.30 which indicates medium resistance towards lateral expansion [9]. The decrease in σ at lower SrO content indicates the increase in actual cross-linking density (Figure 6 (a)) at low SrO content. The conversion to four coordinated boron from three coordinated boron, would strengthen the structure of the glass during initial addition of alkali earth oxide. Higher value in σ at higher SrO content (x ≥ 40 mol%) may be attributed to NBO formation and mixed of crystalline / amorphous phase which resulted in formation of grain / phase boundaries in the samples. Hardness (H) expresses the stress required to eliminate the free volume of the glass which is the openness of the glasses over that of corresponding crystals [26-27]. H is observed to increase with the SrO content at x ≤ 40 mol% (Figure 6 (a)). Increase in H at initial addition of SrO (x ≤ 35 mol%) is related to conversion of boron from triangular to tetrahedral coordination in glass network which strengthens the glass network. Larger drop in H at higher SrO content could be due to combination factors of NBO formation and formation of two phase microstructure with grain/phase boundaries, which weakens the structure of the glass.

Quantitative analysis of elastic properties of xSrO-10PbO-(90-x)B_2O_3 (x = 20-45 mol%) samples were performed using the bulk compression and the ring deformation models. K_{bc}/K_e ratio (Figure 6 (b)) is close to 2 for the samples prepared, suggesting ring deformation along with isotropic elastic deformation as mentioned by Bridge et al. [9]. From the figure, this ratio decreased up to x ≤ 35 mol% which could be due to the decrease in ring deformation which indicates a stronger connection between the structural units and improved structural stablity [10]. It could be noted that the rate of decrease is higher at x = 35 mol% which could further suggest that most of structure in borate glass were converted into diborate group where ring deformation is difficult to occur due to the stronger linkage in these group. This could be confirmed from the FTIR results which showed maximum diborate group concentration at x = 35 mol%. At x > 35 mol%, K_{bc}/K_e ratio was seen to increase. This could be due to the formation of NBO and formation of two phase microstructure with grain/phase boundaries. According to the ring deformation model suggested by Bridge et al. [9], the deformation is not ideally isotropic because some parts of the rings may be deformed due to bending under compression. ℓ was seen to decrease rapidly for x ≤ 35 mol% and it could be due to closer packing in the network as the structure comprises of more tetraborate and

diborate units [27]. With further SrO addition (x > 35 mol%), ℓ was seen to continue decreasing at lower rate and it may due to the competition of NBO formation and closer packing in network due to formation of crystalline phase.

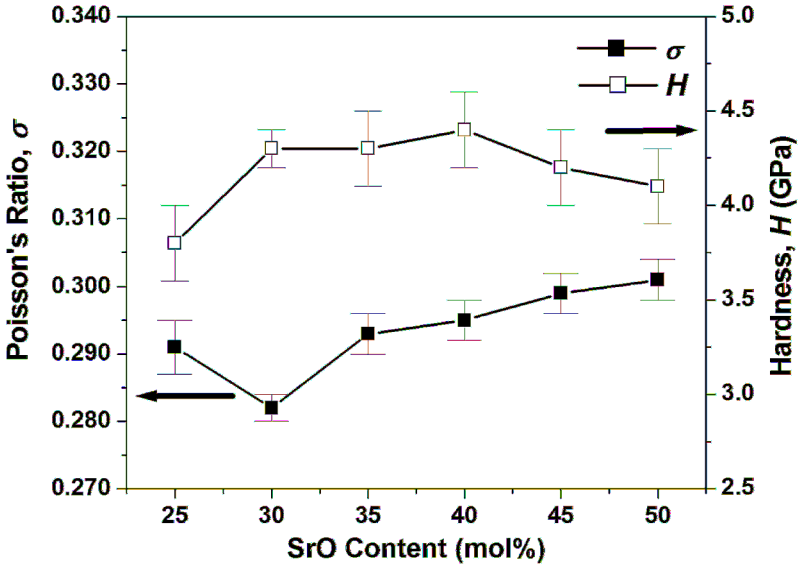

(a)

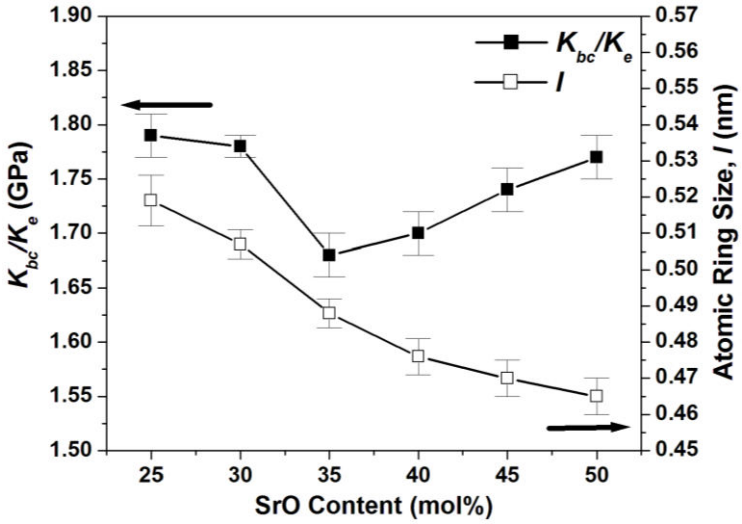

(b)

Figure 6: Plot of (a) Poisson's ratio (σ) and hardness (H) & (b) K_{bc}/K_e ratio (σ) and atomic ring size (ℓ) for $xSrO\text{-}(90\text{-}x)B_2O_3\text{-}2CeO_2\text{-}8Al_2O_3$ (x=25-50 mol%) samples

CONCLUSION

X-ray analysis, FTIR and ultrasonic measurements at room temperature of the xSrO-(90-x)B_2O_3-2CeO_2-8Al_2O_3 (x=25-50 mol%) samples demonstrate that:

1. X-ray data shows the amorphous behavior at x ≤ 35 mol% and mixed crystalline / amorphous phases at x > 35 mol%.
2. Optical image, FESEM image and EDX analysis revealed that the samples contained Ce-rich crystalline phase and Ce depleted glass phases.
3. FTIR confirmed the existence of trigonal and tetrahedral borate groups. The value of N_4, determined from FTIR data, increased at x ≤ 35mol% which revealed that the conversion of BO_3 units to BO_4 units took place dominantly at lower SrO content and NBO formation at higher SrO content.
4. Increase in ultrasonic velocities (v_L and v_S), longitudinal modulus (C_L), shear modulus (μ), bulk Modulus (K), Young's modulus (Y) and hardness (H) at x ≤ 35 mol% indicating an increase in strength of glass which was attributed to the formation of compact four coordinated boron (BO_4) structure. Decrease in ultrasonic velocities and elastic moduli related to combination factors of formation of NBO and formation of grain/phase boundaries due to mixed crystalline/amorphous phases at higher SrO addition.
5. The decrease in K_{bc}/K_e ratio and significant decrease in ℓ, derived from the bulk compression model, indicated decrease in ring deformation in the glass network with the SrO addition within borate anomaly region.

ACKNOWLEDGEMENT

The authors would like to thank Universiti Teknologi MARA for financial support to this research project.

REFERENCES

[1]. S. Krause, C. Pfau, M. Dyrba, P.-T. Miclea, S. Schweizer, *J. Lumin.* **151** 29–33 (2014)
[2]. L. A. E. Latif, *J. Pure Appl. Ultrason.* **27** 80–91 (2005)
[3]. S. Kaur, G. Pal Singh, P. Kaur, D. P. Singh, *J. Lumin.* **143** 31–37 (2013)
[4]. P. Kaur, S. Kaur, G. P. Singh, D. P. Singh, *J. Alloys Compd.* **588** 394–398 (2014)
[5]. I. Pal, A. Agarwal, and S. Sanghi, *Indian J. Pure Appl. Phys.,* **50** 237-244 (2012)
[6]. S. Arunkumar, K. Marimuthu, *J. Alloys Compd.* **565** 104–114 (2013)
[7]. M. M. Umair, A. K. Yahya, M. K. Halimah, H. A. A. Sidek, *J. Mater. Sci. Technol.* **31** 83–90 (2015)
[8]. B. Bridge, A.A. Higazy, *Phys. Chem. Glasses* **27** 1-14 (1986)
[9]. B. Bridge, N. D. Patel, D. N. Water, *Phys. Status Solidi A* **77** 655–668 (1983)
[10]. Y. B. Saddeek, *Mater. Chem. Phys.* **83** 222–228 (2004)

[11]. NIIR Board of Consultants & Engineers, The Complete Book on Glass and Ceramics Technology. Asia Pacific Business Press Inc., Delhi, 2005.
[12]. J. E. Shelby, Introduction to Glass Science and Technology, second ed., Royal Society of Chemistry, Cambridge, 2005.
[13]. P. Pascuta, R. Lungu, I. Ardelean, *J. Mater. Sci. Mater. Electron.* **21** 548–553 (2009)
[14]. B. Sumalatha, I. Omkaram, T. R. Rao, C. L. Raju, *J. Non. Cryst. Solids* **357** 3143–3152 (2011)
[15]. D. Maniu, I. Ardelean, T. Iliescu, S. Cinta, *J. Mol. Struct.* **2860** 291-294 (1997)
[16]. M. Pal, *J. Mod. Phys.* **2** 1062–1066 (2011)
[17]. J. S. Kumar, J. L. Kumari, M. S. Rao, S. Cole, *Opt Mater* **35** 1320–1326 (2013)
[18]. F. A. Moustafa, A. M. Fayad, F. M. Ezz-Eldin, I. El-Kashif, *J. Non. Cryst. Solids* **376** 18–25 (2013)
[19]. C. Gautam, A. K. Yadav, A. K. Singh, *ISRN Ceramics* **2012** 1-17 (2012)
[20]. S. R. Rejisha, N. Santha, *J. Non. Cryst. Solids* **357** 3813–3821 (2011)
[21]. M. Subhadra, P. Kistaiah, *Vib. Spectrosc.* **62** 23–27 (2012)
[22]. A. Rudin, The Elements of Polymer Science and Engineering: An Introductory Text for Engineers and Chemists, Academic Press, New York, 1982.
[23]. J. Roesler, H. Harders, M. Baeker, Mechanical Behaviour of Engineering Materials: Metals, Ceramics, Polymers, and Composites, first ed., Springer, New York, 2007.
[24]. S. Laila, S. N. Supardan, A. K. Yahya, *J. Non. Cryst. Solids* **367** 14–22 (2013)
[25]. M. K. Halimah, W. M. Daud, H. A. A. Sidek, *Ionics (Kiel).* **16** 807–813 (2010)
[26]. N. S. A. B. D. El-Aal, H. A. Afifi, *Arch. Acoust.* **654** 641–654 (2009)
[27]. T. Z. A. M. Hamezan, A. A. Sidek, A. W. Zaidan, K. Kaida, *J. Appl. Sci.* **6** 943–949 (2006)
[28]. H. Bahari, S. A. Aziz, H. M. Kamari, *J. Ceram. Soc. Jpn.* **120** 280-285 (2012)